Hybrids of glass fibers coated with carbon nanotubes and nickel for high-performance electromagnetic wave absorption composites

Yu Liu, Delong He, Olivier Dubrunfaut, Anne Zhang, Lionel Pichon, Jinbo Bai

Hybrids of glass fibers coated with carbon nanotubes and nickel for high-performance electromagnetic wave absorption composites

Yu LIU[1,2,3,4], Delong HE[4]*, Olivier DUBRUNFAUT[5], Anne ZHANG[4], Lionel PICHON[5]*, Jinbo BAI[4]

1 Powder Metallurgy Research Institute, Central South University, 410083 Changsha, PR China

2 State Key Laboratory of Powder Metallurgy, Central South University, Changsha, Hunan 410083, China

3 Hunan Province Key Laboratory of New Specialty Fibers and Composite Material,

Central South University, Changsha, Hunan 410083, China

4. Université Paris-Saclay, CentraleSupélec, CNRS, Laboratoire de Mécanique des Sols, Structures et Matériaux (MSSMat), 91190, Gif-sur-Yvette, France

5. Université Paris-Saclay, CentraleSupélec, CNRS, Sorbonne Université, Laboratoire Génie électrique et électronique de Paris (GeePs), 91190, Gif-sur-Yvette, France

*** Corresponding author:**

Dr. Delong He, Email: delong.he@centralesupelec.fr.

Prof. Lionel Pichon, Email: lionel.pichon@centralesupelec.fr

Abstract

To expand the application of insulating glass fiber (GF) in the field of microwave absorption, one type of glass fibers (GF) hybrids with carbon nanotubes (CNTs) and nickel (Ni) was successfully synthesized by chemical vapor deposition (CVD) and electroless plating methods. By changing the reaction conductions, the morphology of GF hybrids including CNT's length, CNT's growth density, and Ni's thickness could be adjusted. The as-produced hybrids were used as multifunctional reinforcement to fabricate epoxy composites. The dielectric properties of composites were particularly measured from 1 to 18 GHz. It was found that the variation of GF hybrids structure significantly changed the dielectric properties of the composites in the tested frequency range. Furthermore, the analytical simulation work based on the experimental results was conducted for optimizing the structural parameters of multilayered composites. The results showed that the best reflection loss of -60dB with a -10dB range of 5.6GHz could be obtained in an absorber with a triple-layered structure composed by GF-CNTs/epoxy with different CNT contents and GF-CNTs@Ni/epoxy. Thus, the proposed hybrid method might be quite efficient for developing composites that can achieve high-performance electromagnetic absorbing.

1 Introduction

Electromagnetic (EM) absorbers have attracted intensive research attention due to the rapid development of electronic devices [1-3]. Many electronic devices are equipped with EM absorbers to reduce interference with the others and also to protect human health from the potential EM radiation [4,5].

According to the processing technology and structural-load-carrying capacity, EM absorbers can be divided into two categories. One type is surface coating materials, including various absorbing coatings or patch ones, such as carbonaceous fillers (e.g. graphene [6], carbon nanotube (CNT) [7,8], carbon black [9-11], dielectric or magnetic materials (e.g. ferrites or titanates), and their hybrids [12-16]. The other type is structural EM absorbing materials. This type does not occupy additional weight and simultaneously has the function of bearing, which is extremely attractive for some fields like aerospace that ask for both lightness and strength. The representative fibers used in this type are carbon fibers (CF) and silicon carbide fibers (SiC_f) [17,18]. However, their costs are very high. Moreover, the EM absorbing properties are limited by their physical properties: for instance, the high electrical conductivity of CF will partially reflect EM wave that consequently reduces the EM wave absorption level [19]. Alternately, glass fiber (GF) has also been widely used as structural composite reinforcement because of its good mechanical properties, low density, and low price [20]. Although GF is an isolated material, high-performance structural absorbing composites can also be achieved by surface treatment on GF or adding absorbing materials into the epoxy matrix. Many works have been reports in this field. Kwak et al. used electroplating to deposit nickel on the surface of GF, and the prepared composite material had an effective absorption bandwidth (EAB, Reflection loss≤-10dB) of 12.2GHz (5.8-18GHz) [21]. Huang et al. prepared a GF and CF reinforced multilayer composite material with an EAB of 16.31GHz (3.42-19.73GHz) when it is only 3.5mm [22]. Chen et al. mixed CNTs and ferro-ferric oxide nanoparticles into GF reinforced composite materials to prepare a double-layered composite. The EAB could cover the entire X-band (8.2-12.4 GHz) and its maximum reflection loss can reach -45.7dB [23]. These results have indicated that the combination of GF and conductive fillers can be an effective alternative to achieve high EM absorbing performance. In the conductive fillers, CNTs have been widely applied in the EM wave absorbing materials because of their high conductivity and compatibility with polymer matrix [24,25].

However, due to the strong Van der Waals forces, CNTs are easy to aggregate and difficult to be uniformly dispersed in the matrix [26]. In our previous work, we have reported a hybrid where CNTs grow directly on the surface of fibers, which has been a promising method to improve the CNT dispersion in the matrix [27,28].

In this work, to further improve the EM absorbing performances of GF reinforced composites, the surface treatments, i.e., the combination of growing CNTs and depositing nickel layers (Ni) (GF-CNTs and GF-CNTs@Ni), will be conducted on the surface of GF to prepare hybrids with core-shell structure. Then two kinds of composites with GF-CNTs and GF-CNTs@Ni have been fabricated and the dielectric properties from 1-18 GHz will be investigated. By changing the reaction conductions, the morphology of GF hybrids including CNT's length, CNT's growth density, and Ni's thickness can be adjusted which can allow us to study the effects of CNT and Ni on the dielectric properties and absorption performance of the composites. Additionally, based on the obtained experimental results, a simulation work based on the experimental results has also been conducted for designing an absorber with a triple-layered structure (the combination of impedance, absorption, and reflection layers) to achieve high EM absorption performances.

2 Experiment

2.1 Sample preparation

The GF-CNTs hybrid was prepared by a floating catalyst CVD method, which was described in our previous work [29]. Briefly, the growth temperature was about 600−750 °C in a mixed atmosphere of argon and hydrogen. Acetylene was used as the carbon source. Ferrocene was used as the catalyst precursor. The growth time lasted 5−10 min. The nickel layer was deposited on the GF-CNTs surface for 10 and 30 min at 45ºC, respectively [30]. The epoxy resin 1080S and a curing agent 1084 were used to fabricate the composites. More details can be found in the reference [29].

2.2 Characterizations

Thermogravimetric analysis (TGA) was conducted on NETZSCH STA 449 F3 with a mixture atmosphere of oxygen and nitrogen. The temperature was raised from room temperature to 900 ºC at a speed of 10 ºC/min. Scanning electron microscopy (SEM, LEO 1530 Gemini) was used to characterize the morphology and microstructure of the samples. The dielectric properties of the specimens were measured by a port network analyzer (PNA-E8364C) in the frequency range of 1GHz to 18 GHz.

3 Results and discussion

The weight fraction of CNTs grown on GFs has a large influence on the electrical property of composites. In this work, the weight fraction of CNTs was modulated by changing their length and grown density, which could be controlled by adjusting the CVD conditions. The TGA was conducted from room temperature to 900 ºC in an oxidation atmosphere to evaluate the mass ratio of CNT grown on GF, as shown in Figure 1. In an oxidation atmosphere, the CNTs start to decompose at about 430 ºC. However, the GF was stable in the tested temperature range. Hence, the mass loss that happened in the TGA was considered as the CNT content grown on the GF. When the CVD growth time changed from 0 to 10 min, the weight fraction of CNT varied from 0% to 0.5%, 1.5%, and 3%, respectively. For the 0.5wt% GF-CNTs, it was synthesized at 600 ºC for 5min and its TGA curve showed lower decomposition temperature than others. This is mainly due to the relatively low CVD temperature used for CNT growth.

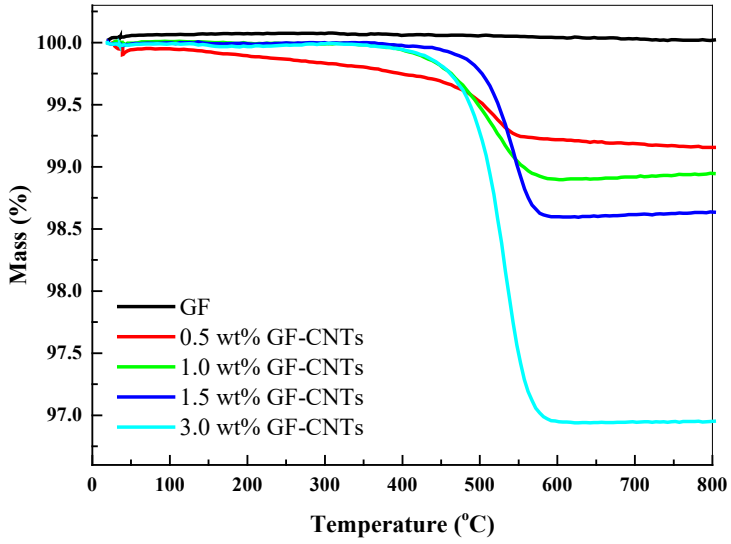

Figure 1 TGA curves of pristine GF and GF-CNTs.

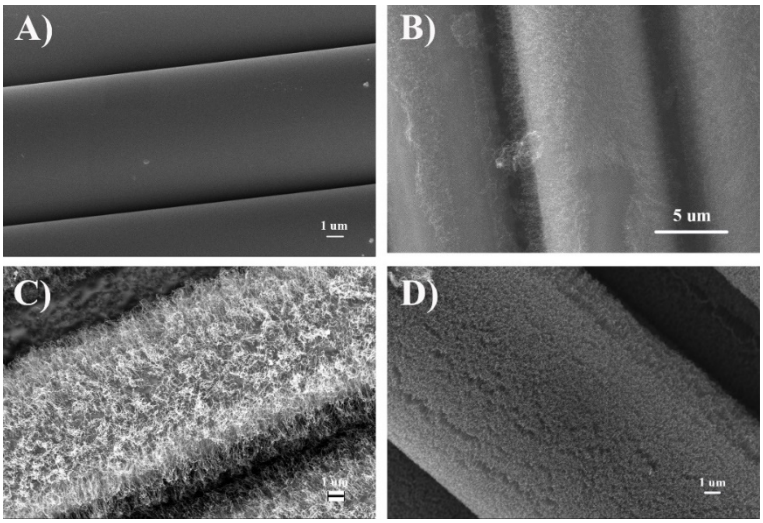

Figure 2 SEM images (A) pristine GF and the GF-CNTs with different CNT mass ratio: (B) 0.5 wt% CNTs; (C) 1.5wt% CNTs; (D) 3.0wt% CNTs.

Figure 2 showed the morphologies of the original GF and the GF-CNTs with different CNT mass ratios. The diameter of the original GF was about 9 μm (**Figure 2A**). After growing 0.5 wt% nanotubes, the smooth surface of GF was completely covered by CNTs and formed a core-shell structure. The diameter increased to 11.26 μm (**Figure 2B**). After increasing the growth time, the CNTs became longer, leading to a larger diameter for GF-CNTs with a high mass ratio (**Figure 2C** and **2D**). When the CNT mass ratio was 1.5 wt% and 3.0 wt%, the apparent diameter of hierarchical GF-CNTs was around 13.61 and 15.65 μm, indicating that the CNT length was 2.2 and 3.2 μm, respectively.

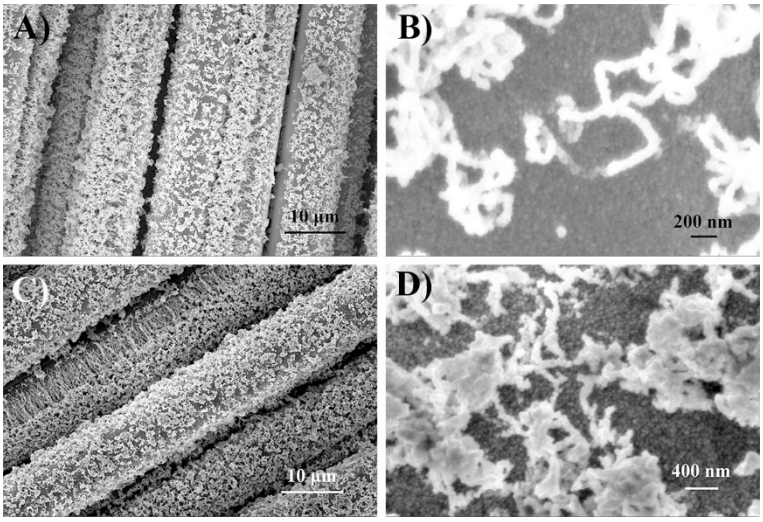

Figure 3 SEM images of (A) and (B) GF-CNTs coated with nickel layer for 10 min with different magnifications; (C) and (D) GF-CNTs coated with nickel layer for 30 min with different magnifications.

The nickel layer deposition was achieved by three steps in the solution. To decrease the detachment of CNTs from GF surface, all the process was conducted by gentle vibration. After 10 min deposition, as shown in **Figure 3(A)**, most of the CNTs were still on the GF surface, and meanwhile, a Ni layer was homogeneously deposited on the surface of GF and CNTs, named as GF-CNTs@Ni-10min. This structure could be figured out in the enlarged SEM image, as shown in **Figure 3(B)**, the surface of GF was completely covered by small Ni particles. This morphology was different from the smooth surface of neat GF as indicated in Figure 2. Moreover, after the deposition, CNTs did not agglomerate with each other; instead, the adjacent CNTs were connected by Ni particles and formed a conductive network. To increase the amount of nickel, the deposition time was increased to 30 min, named as GF-CNTs@Ni-30min, as shown in **Figure 3(C)**. More CNTs were detached from the GF surface comparing to those of GF-CNTs@Ni-10min. The nickel layer was homogeneous. More CNTs were covered by Ni particles and some aggregates of CNT and Ni were formed on the GF surface (**Figure 3(D)**).

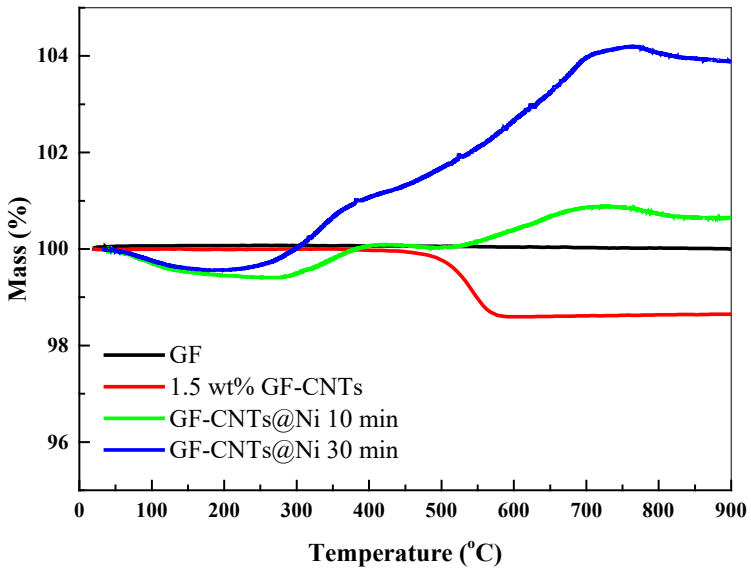

Figure 4 TGA curves of original GF, GF-CNTs, and GF-CNTs@Ni with different deposition times.

The content of the nickel layer on the hybrid was estimated by TGA and the results are shown in **Figure 4**. There was almost no mass loss from room temperature to 900ºC for the original GF. The TGA curve

of 1.5wt% GF-CNTs was also shown in the figure to make a comparison. CNTs began to decompose at around 500 ºC. The final mass loss was about 1.5%. For the GF-CNTs@Ni-10min, there was a small mass loss of about 0.5% at 200ºC, which could attribute to the decomposition of a small amount of ammonium chloride or other pH buffers contained in the nickel layer. After 200 ºC, the mass began to increase, which was mainly caused by the oxidation of the nickel layer. The mass increases slowly from 400 ºC to 500 ºC. The mass loss caused by the decomposition of carbon nanotubes and the mass gain caused by oxidation of the nickel layer was offset by each other. Beyond 500 ºC, the carbon nanotubes have been completely decomposed and the rate of mass gain accelerated. The mass tended to be stable when it reached 800 ºC. Therefore, the mass gain caused by the oxidation of nickel was about 1.2%. If the nickel oxides were NiO, the nickel content in GF-CNTs@Ni-10min was about 4.4%. For the GF-CNTs@Ni-30min, the nickel content was about 15.8%. However, nickel oxides include NiO and Ni_2O_3. The actual nickel content may be lower than the estimated one.

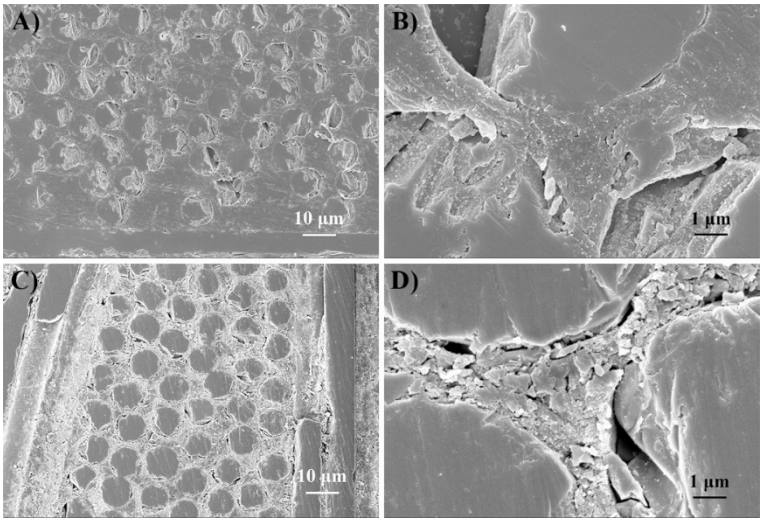

Figure 5 SEM images of the cross-section of the composites: (A) and (B) 1.5wt% GF-CNTs/epoxy; (C) and (D) GF-CNTs@Ni 30 min/epoxy composite.

To investigate the electrical behaviors of the GF-CNTs and GF-CNTs@Ni reinforced epoxy composites, the microstructures of the composites were characterized by SEM, as shown in Figure 5. The cross-section was obtained by polishing the fracture surface with low speed to reduce the damage of the original morphology. Figure 5(A) showed the cross-section of 1.5 wt% GF-CNTs/epoxy composite. The

cross-section showed good quality, few defects can be found in the images. After zooming in the interface region of composites, as shown in Figure 5(B), a distinguished annular region surrounded each GF, named interphase. As the length of CNTs increasing, the thickness of the interphase increased progressively, which helped form the conductive network in the matrix. However, the improvement of the electrical performance of the composite by the CNTs modified GF was very limited. In the process of preparing the composite, the CNTs were easy to fall off the surface of the fiber, and it was difficult to maintain its original structure. In addition, the improvement of electrical performance mainly depends on the overlapping of carbon nanotubes. However, GF is insulated, and the contact resistance between carbon nanotubes was very large. Therefore, a nickel layer was deposited on the surface of the hybrid, which helped the CNTs and GF surface form a complete conductive network, improving the electrical properties of the composite. As shown in **Figure 5C**, the nickel layer and the CNTs increased the conductivity of the matrix between the fibers. **Figure 5D** showed a connection area between the fiber and the matrix. The CNTs wrapped by the nickel layer were evenly dispersed in the matrix.

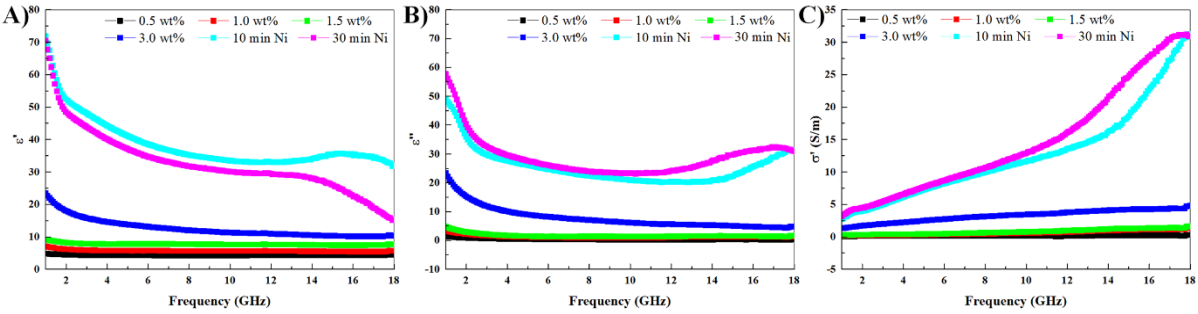

Figure 6 Frequency dependence of complex permeability and conductivity spectra for GF-CNTs/epoxy and GF-CNTs@Ni/epoxy composites: (A) real part permittivity (ε'), (B) imaginary part permittivity (ε''), and (C) conductivity (σ').

The microwave absorption performance was determined by the dielectric properties of the composites. **Figure 6 (A) and (B)** showed the dielectric properties of the composites in the frequency range of 1–18 GHz. The values of ε' and ε" in 0.5 wt% GF-CNTs/epoxy composite were about 4.3 and 0.2, respectively. They were very stable in the tested range. Both ε' and ε" increased following the increase of the weight percentage of CNT content in the composites. The maximum ε' and ε" values of GF-CNTs/epoxy

composites appeared at low frequency (1GHz) corresponding to CNT content of 1.0 and 1.5% are 7.06 and 9.21 for ε', 3.35 and 4.79 for ε", respectively. A large improvement of the permittivity was observed when CNT content was 3.0%, achieved 23.45 for ε' and 23.38 for ε", respectively. As the mass ratio of CNTs increased, the length and growth density of CNTs on the GF also increased, which contributed to the construction of the conductive network. After deposited nickel on the hybrids for 10 min, the permittivity was greatly increased, 71.85 for ε' and 49.02 for ε", respectively. When the deposition time was extended to 30 minutes, although the nickel layer became thicker, the dielectric permittivity has not increased significantly. This is mainly because the longer time in the solution results in the carbon tubes falling off from the fiber so that the increase in the dielectric permittivity was limited. In addition, the conductive network has been established, and further increasing the nickel content was not very useful for improving the conductivity. **Figure 6(C)** showed the frequency dependent AC conductivity. The conductivity was then deduced:

$$\sigma_{AC} = \sigma'(\omega) = \varepsilon_0 \varepsilon'' \omega \qquad (1)$$

The conductivity tended to increase as the frequency increased. The same tendency can be found as permittivity. Therefore, the electrical conductivity of the composites could be modulated by growing CNTs on the GF surface at a very wide range.

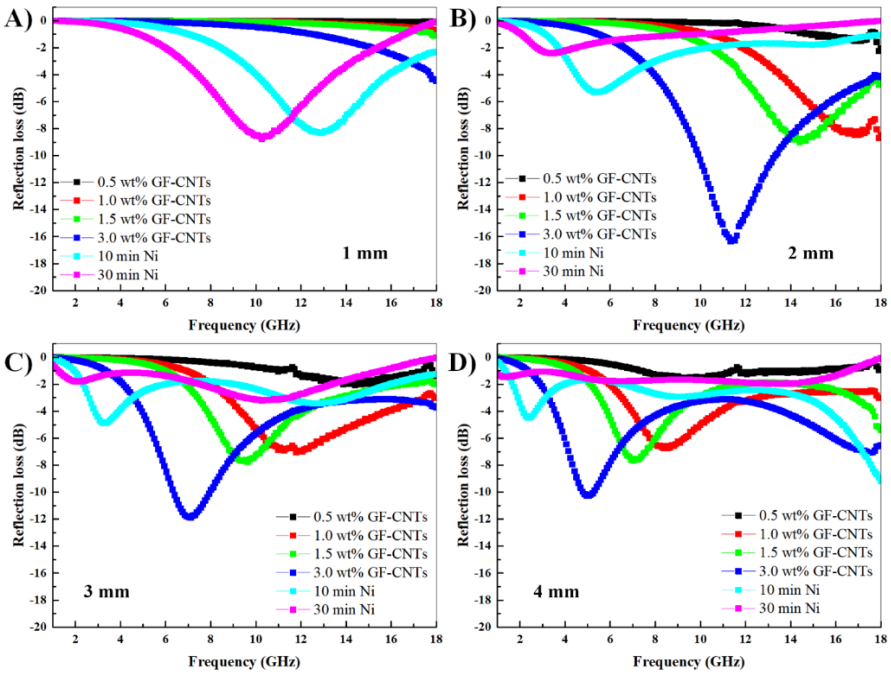

Figure 7 Reflection loss curves for different thicknesses of GF-CNTs/epoxy and GF-CNTs@Ni/epoxy composites: (A) 1 mm, (B) 2 mm, (C) 3 mm, and (D) 4 mm.

The transmission line theory was employed to calculate the theoretical reflection loss values of the composites. The reflection loss of a single-layer absorber can be calculated by the following equation [31]:

$$RL(dB) = 20\log\left|\frac{Z_{in}-Z_0}{Z_{in}+Z_0}\right| \qquad (2)$$

Figure 7 showed the frequency dependence of reflection loss in the range of 1–18 GHz for GF-CNTs/epoxy composites with CNTs% of 0.5, 1.0, 1.5, and 3 wt% and GF-CNTs@Ni/epoxy with different deposition times, respectively. As indicated by Figure 7(A), it could be found that the GF-CNTs/epoxy composites exhibited weak microwave absorption properties across the whole frequency range. The absorption property was enhanced by incorporating nickel on the GF-CNTs surface, which reached -8 dB for both GF-CNTs@Ni/epoxy composites. As the thickness increased to 2 mm, the samples showed better microwave absorption properties and the peak values moved to lower frequency as the CNT content increasing, -2.2 dB (18GHz), -8.3 dB (16.7GHz), -9 dB (14.4 GHz), and -16.4 dB (11.3 GHz) for the samples with CNTs% of 0.5, 1.0, 1.5, and 3.0wt%, respectively. The EAB was only observed for the composites with CNT content at a high fraction, 10.0-13.2 GHz for 3.0 wt%. The GF-CNTs@Ni/epoxy composites showed worse absorption property at 2mm and the absorption peak was shifted to low frequency, -5.3 dB(5.4GHz) and -2.4 dB(3.2GHz), respectively. A possible reason was that the improved conductivity by the nickel layer could lead to the impedance mismatching of the material and the air and resulting in the reduction of the wave absorbing performance. As the thickness of the sample increased to 3 mm, the absorption properties had no obvious change. However, the absorption peaks moved to lower frequency, -2.0 dB (14.4GHz), -7.0 dB (11.8GHz), -7.7 dB (9.4GHz) and -11.9 dB (7.1 GHz) for the samples with CNT content of 0.5, 1.0, 1.5 and 3.0wt%, respectively. The EAB became smaller compared with those of the 2 mm samples, 6.4-7.9 GHz for 3.0 wt%. As the thickness of the sample further increasing to 4mm, the absorption properties were decreased, and the

peak values continued to shift to a lower frequency. The absorption tendency was the same as other thicknesses. The best performance was the GF-CNTs/epoxy with a CNT content of 3.0wt%.

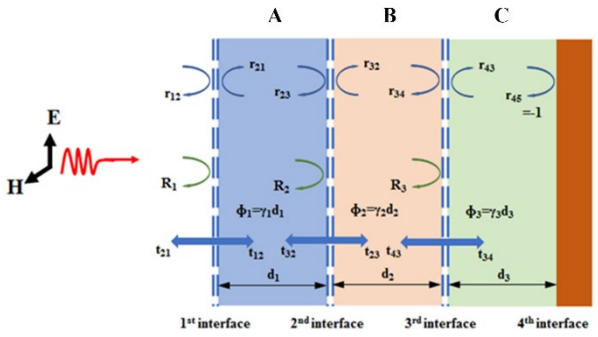

Figure 8 Triple-layered electromagnetic wave absorber.

It could be found that for single-layered GF-CNTs/epoxy or GF-CNTs@Ni/epoxy composites, the minimum reflection loss and EAB were limited. For GF-CNTs/epoxy composites, the absorbing mechanism mainly could be attributed to the improved ε" because of the formation of a conductive network composed of CNTs. For the GF-CNTs@Ni/epoxy composite material, due to the existence of Ni, the improvement in electrical conductivity led to the impedance mismatch. Hence, more EM waves have been reflected rather than absorbed. To further enhance the absorption performance, a triple-layered structure has been designed, as shown in **Figure 8**. The reflection coefficient of each layer could be expressed as [32,33]

$$R_1 = r_{12} + \frac{t_{21}t_{12}R_2e^{-2i\Phi_1}}{1-r_{21}R_2e^{-2i\Phi_1}} \quad (3)$$

$$R_2 = r_{23} + \frac{t_{32}t_{23}R_3e^{-2i\Phi_2}}{1-r_{32}R_3e^{-2i\Phi_2}} \quad (4)$$

$$R_3 = r_{34} + \frac{t_{43}t_{34}r_{45}e^{-2i\Phi_2}}{1-r_{43}r_{45}e^{-2i\Phi_2}} \quad (5)$$

And the reflection loss of triple-layered structure could be expressed as

$$R_L = -20\lg|R_1| \quad (6)$$

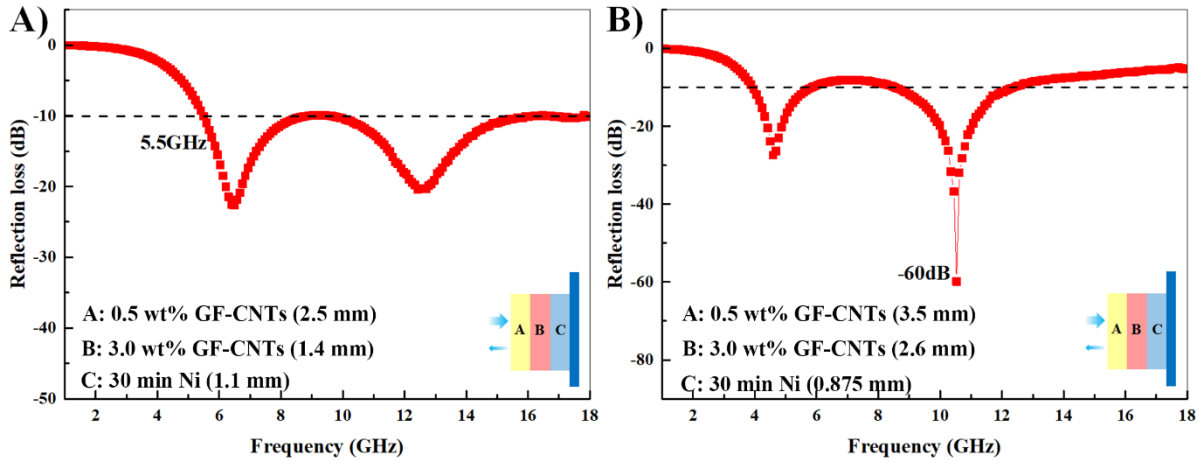

Figure 9 The RL values of the optimized triple-layered structures.

Based on the obtained experimental results, it can be concluded that a multi-layered structure, which contains the impedance layer, the absorption layer, and the reflection layer, can largely improve the microwave absorption performance. In this work, the 0.5 wt% and 3.0 wt% GF-CNTs/epoxy composites were used as the impedance layer and the absorption layer, respectively. The 30min GF-CNTs@Ni/epoxy composite was used as the reflection layer due to the high conductivity. A reflection loss of -23 dB and the -10 dB range of 12.5 GHz (5.5-18 GHz) can be obtained by using 2.5mm 0.5 wt% GF-CNTs/epoxy, 1.4mm 3.0 wt% GF-CNTs/epoxy and 1.1mm GF-CNTs@Ni 30min/epoxy composites, as shown in **Figure 9A**. When the thickness of 0.5 wt% GF-CNTs/epoxy increased to 3.5 mm, the thickness of 3.0 wt% GF-CNTs/epoxy increased to 2.6 mm, and the thickness of GF-CNTs@Ni 30min/epoxy was 0.875 mm, the absorption peak increased to about -60 dB, as shown in **Figure 9B**. In this study, the 0.5wt% GF-CNTs/epoxy was chosen as the air contact layer because of its good impedance matching characteristic. As mentioned above, 0.5wt% GF-CNTs had relatively short, sparse carbon nanotubes, which could partially improve the dielectric properties of the composite and simultaneously maintain an impedance close to that of the air. Hence, it can be easier to meet the impedance matching requirements and achieve higher EM wave absorption. For the absorption layer, we selected the 3.0wt% GF-CNTs/epoxy. The long carbon nanotubes and high growth density made it easier to form a conductive network, resulting in a higher ε''. At the same time, the EM waves could also be dissipated by multiple reflecting and scattering between carbon nanotubes. The GF-CNTs@Ni

30min/epoxy was chosen as the reflection layer because of the high conductivity by depositing Ni. Thereby, the reflected EM waves can be re-absorbed by the absorbing layer. The results were also compared with other reported CNT-based materials, which have the compatible advantages of the low RL peak value, broad absorption bandwidth and thin thickness (Table 1).

Table 1 Some recent studies of the GF reinforced polymer composites for absorption application.

Composites	**Layers**	**Fillers**	**RL (dB)**	**Bandwidth (GHz) (<-10 dB)**	**Thickness (mm)**	**Reference**
GF/epoxy	Double	CNTs	-30	4.2	3.1	[34]
CF/GF/epoxy	Double	CF@Ni	-48.1	3.2	2.5	[5]
GF/epoxy	Double	CNTs+Fe_3O_4	-45.7	4.2	1.8	[23]
GF/epoxy	>3	Graphene	-30	10	3.8	[35]
GF-CNTs(@Ni)/epoxy	Triple	GF-CNTs+GF-CNTs@Ni	-23 -60	12.5 5.6	5 ~7	This work

Conclusion

In this work, multifunctional GF hybrids were successively developed by by growing vertically aligned CNTs and coating nickel layers. The experimental results showed that the EM properties of the hybrid composites could be adjusted by a number of factors, such as the CNT's length, its growth density, and the thickness of the deposited nickel layer, which provided the possibility for optimizing structural parameters of composites for designing absorbers with high-performance. The 3.0 wt% GF-CNTs/epoxy composite with a thickness of 2mm showed a reflection loss of -16 dB and a wide -10 dB range (5.3GHz). A reflection loss of -60dB with a -10dB range of 5.6GHz (3.9-5.77GHz and 8.5-12.3GHz) was further obtained in the triple-layered structure, which was composed oftwo GF-CNTs/epoxy composites with different CNTs contents and one GF-CNTs@Ni/epoxy. The -10dB range could further be expanded to 12.5GHz (5.5-18GHz) by changing the thickness of each component. The simulation results showed that an absorber with a multi-layered structure could be efficient in EM absorption application.

Acknowledgement

This work has benefited from the financial support of the LabEx LaSIPS, France (ANR-10-LABX-0032-LaSIPS) managed by the French National Research Agency under the “Investissements d’avenir” program (ANR-11-IDEX-0003).

References

1. Kong, H. X., Current Opinion in Solid State and Materials Science 17, 31 2013.
2. Wu, X.; Mu, F.; Zhao, H., Journal of Materials Science & Technology 55, 16 2020.
3. Fan, W.; Yuan, L.; D'Souza, N.; Xu, B.; Dang, W.; Xue, L.; Li, J.; Tonoy, C.; Sun, R., Polymer Testing 69, 71 2018.
4. Song, W.-L.; Zhang, K.-L.; Chen, M.; Hou, Z.-L.; Chen, H.; Yuan, X.; Ma, Y.; Fang, D., Carbon 118, 86 2017.
5. Chen, W.; Peng, K.; Wang, J.; He, X.; Su, Y.; Zhang, B.; Su, X., Materials Research Express 6, 126324 2020.
6. Zhi, D.; Li, T.; Li, J.; Ren, H.; Meng, F., Composites Part B: Engineering 211, 108642 2021.
7. Zhang, M.; Qian, X.; Zeng, Q.; Zhang, Y.; Cao, H.; Che, R., Carbon 175, 499 2021.
8. Wang, Y.-Y.; Zhou, Z.-H.; Zhou, C.-G.; Sun, W.-J.; Gao, J.-F.; Dai, K.; Yan, D.-X.; Li, Z.-M., ACS Applied Materials & Interfaces 12, 8704 2020.
9. Kumar, R.; Sahoo, S.; Joanni, E.; Singh, R. K.; Tan, W. K.; Kar, K. K.; Matsuda, A., Carbon 177, 304 2021.
10. Akinay, Y.; Hayat, F.; Kanbur, Y.; Gokkaya, H.; Polat, S., Polymer Composites 39, E2143 2018.
11. Anand, S.; Pauline, S., Advanced Materials Interfaces 8, 2001810 2021.
12. Li, W.; Zhang, J.; He, D.; Wang, G.; Wang, T., Journal of Physics D: Applied Physics 54, 305002 2021.
13. Pei, X.; Zhao, M.; Li, R.; Lu, H.; Yu, R.; Xu, Z.; Li, D.; Tang, Y.; Xing, W., Composites Part A: Applied Science and Manufacturing 145, 106363 2021.
14. Pan, Y.; Wang, C.; Dong, H.; Ma, G.; Li, N.; Liu, C.; Wang, J.; Jian, X., Journal of Alloys and Compounds 865, 158708 2021.
15. Huang, Z. D.; Ma, R.; Zhou, J.; Wang, L.; Xie, Q., Journal of Alloys and Compounds 873, 159779 2021.
16. Ding, L.; Zhao, X.; Huang, Y.; Yan, J.; Li, T.; Liu, P., Journal of Colloid and Interface Science 595, 168 2021.
17. Zhou, J.; Li, Y.; Zhang, M.; Xu, E.; Yang, T., Materials Today Communications 26, 101960 2021.
18. Kwon, H.; Jang, M.-S.; Yun, J.-M.; Park, Y.; Shin, C.; Yang, J.; Kim, C.-G., Composite Structures 261, 113286 2021.
19. Hong, J.; Xu, P.; Xia, H.; Xu, Z.; Ni, Q.-Q., Composites Science and Technology 203, 108616 2021.
20. Sathishkumar, T.; Satheeshkumar, S.; Naveen, J., Journal of Rnforced Plastics & Composites 33, 1258 2014.
21. Kwak, B.-S.; Jeong, G.-W.; Choi, W.-H.; Nam, Y.-W., Composite Structures 256, 113148 2021.
22. Huang, Y.; Yuan, X.; Chen, M.; Song, W.-L.; Chen, J.; Fan, Q.; Tang, L.; Fang, D., Carbon 144, 449 2019.
23. Chen, W.; Zheng, X.; He, X.; Su, Y.; Wang, J.; Yang, J.; Chen, S.; Zheng, Z., Polymer Testing 86, 106448 2020.
24. Sun, Q.; Zhang, X.; Liu, R.; Shen, S.; Wu, F.; Xie, A., Synthetic Metals 272, 116644 2021.
25. Zhang, H.; Pang, H.; Duan, Y.; Zhang, W.; Wang, T.; Zhang, X., Journal of Materials Science: Materials in Electronics 32, 12208 2021.
26. Wu, C.; Wu, R.; Tam, L.-h., Nanotechnology 32, 325705 2021.
27. He, D.; Salem, D.; Cinquin, J.; Piau, G.-P.; Bai, J., Composites Science and Technology 147, 107 2017.

28. He, D.; Fan, B.; Zhao, H.; Lu, X.; Yang, M.; Liu, Y.; Bai, J., ACS Applied Materials & Interfaces 9, 2948 2017.
29. Liu, Y.; He, D.; Dubrunfaut, O.; Zhang, A.; Pichon, L.; Bai, J., Applied Composite Materials2021.
30. Lee, J.; Jung, B. M.; Lee, S. B.; Lee, S. K.; Kim, K. H., Applied Surface Science 415, 99 2017.
31. Park, K.-Y.; Lee, S.-E.; Kim, C.-G.; Han, J.-H., Composites Science and Technology 66, 576 2006.
32. Thompson, R. C., Journal of Modern Optics 37, 147 1990.
33. Amin, M.; Farhat, M.; Bağcı, H., Opt. Express 21, 29938 2013.
34. Lee, S.-E.; Kang, J.-H.; Kim, C.-G., Composite Structures 76, 397 2006.
35. Marra, F.; Lecini, J.; Tamburrano, A.; Pisu, L.; Sarto, M. S., IEEE Transactions on Microwave Theory and Techniques 68, 590 2020.